

22. GEOCHEMISTRY, MINERALOGY, AND ^{40}K - ^{40}Ar RADIOMETRIC DATING OF LEG 84 BASALTS—GUATEMALA TRENCH¹

H. Bellon, and R. C. Maury, Université de Bretagne Occidentale,
and

J. L. Joron, J. Bourgois, and J. Aubouin, Université Pierre et Marie Curie²

ABSTRACT

Geochemical (atomic absorption, neutron activation analyses), mineralogical (microprobe), and radiometric (^{40}K - ^{40}Ar) data are presented for five basalts from the Guatemala Trench area (Deep Sea Drilling Project, Leg 84).

Strong geochemical and mineralogical differences distinguish two types among these basalts: (1) One basalt (Sample 567A-19,CC), recovered below Upper Cretaceous limestone has the following characteristics: it is quartz normative and has low TiO_2 content, as well as low amounts of Cr, Ni and other transition metals, an LREE depleted pattern, and affinities of clinopyroxene phenocryst plotted into the field of tholeiitic and calc-alkalic pyroxenes. (2) Four alkaline basalts, recovered from the mafic and ultramafic acoustic basement, are nepheline normative and show high TiO_2 content, high amounts of Cr, Ni and so on, an LREE enriched pattern and compositions of clinopyroxene phenocryst plotted close to or within the field of alkali basalt pyroxenes. These basalts are comparable to those recognized in the lower part of the Santa Elena complex and are clearly different from the oceanic basalts of the Cocos Plate.

The radiometric age of the orogenic basalt seems to be close to 80 Ma. The alkaline basalts are clearly older, even if a discrepancy appears between the results of different analyses because of the secondary effects of alteration.

INTRODUCTION

Hole 567A was drilled only 100m from Hole 494A (DSDP Leg 67, Fig. 1). From the top to the bottom, the following succession was encountered: (1) Pleistocene and Pliocene slope sediments; (2) Miocene sediments; (3) Upper Cretaceous (upper Campanian - lower Maestrichtian) limestones; and (4) an acoustic basement of mafic and ultramafic rocks (Bourgois et al., this volume). A few pieces of basalt were recovered from this hole; five of these have been studied with one major goal—to determine their possible affinities with the Leg 67 basalts (Maury et al., 1982) by identifying their magmatic parentages and their ^{40}K - ^{40}Ar ages.

LITHOLOGY

Sample 567A-19,CC is a core-catcher sample recovered below Upper Cretaceous limestones; its stratigraphic position is similar to that of the andesitic samples recovered from the bottom of Hole 494A, DSDP Leg 67. This porphyritic basalt contains millimetric phenocryst of altered olivine as well as fresh calcic clinopyroxene in a microlitic groundmass consisting of plagioclase, clinopyroxene, and titanomagnetite; the residual glass has been converted to chlorite and calcite.

The few other samples (567A-25-2, 90–96 cm; 567A-25-3, 74–78 cm; 567A-26-1 (Piece 1, 3–4 cm) and 567A-29-2, 147–149 cm represent basaltic blocks that are con-

sidered to be tectonically emplaced in the mafic and ultramafic plutonic basement (Bourgois et al., this volume). Sample 567A-26-1 (Piece 1, 3–4 cm) shows a progressive transition from a texture made of skeletal microlites of plagioclase and clinopyroxene to one composed of a fine-grained doleritic texture. This observation suggests that this block could be interpreted to be a pillow fragment. This sample probably represents the outer boundary (quenched facies) and the inner unquenched boundary of a pillow. Sample 567A-29-2, 147–149 cm shows a quenched texture. Finally, Samples 567A-25-2, 90–96 cm and 567A-25-3, 74–78 cm are coarse-grained dolerites.

These four samples contain phenocrysts of altered olivine, fresh clinopyroxene and plagioclase in a groundmass consisting of plagioclase, clinopyroxene, titanomagnetite, and hemoilmenite. Alteration minerals (see radiometric section) are also present, consisting of abundant chlorite and calcite in all samples analyzed as well as celadonite and albite in the groundmass of Sample 567A-26-1 (Piece 1, 3–4 cm) (Table 5).

CHEMISTRY

Major Elements

Sample 567A-19,CC is a quartz normative (1%) basalt with low TiO_2 (0.64 wt. %) and high Al_2O_3 (16.41 wt. %) contents (Table 1). These results are similar to those obtained for the stratigraphically equivalent basalts and andesites from Hole 494A (Maury et al., 1982; Table 1). Chemically, the four other samples seem very similar and contrast strongly with Sample 567A-19,CC. They have a low SiO_2 content (42.3 to 46.1 wt. %) and a high TiO_2 content (2.3 to 2.6 wt. %). Three are nepheline normative basalts; the fourth is silica oversaturated

¹ von Huene, R., Aubouin, J., et al., *Init. Repts. DSDP*, 84: Washington (U.S. Govt. Printing Office).

² Addresses: (Bellon and Maury) Université de Bretagne Occidentale, GIS "Océanologie et Géodynamique" No. 410012, Avenue Le Gorgeu, 29283 Brest Cédex, France; (Joron) Groupe des Sciences de la Terre, Laboratoire de Pierre Sûte, CEN Saclay BP2, 91190 Gif-sur-Yvette, France; (Bourgois and Aubouin) Département de Géotectonique, Université Pierre et Marie Curie, 4, Place Jussieu, 75230 Paris, France.

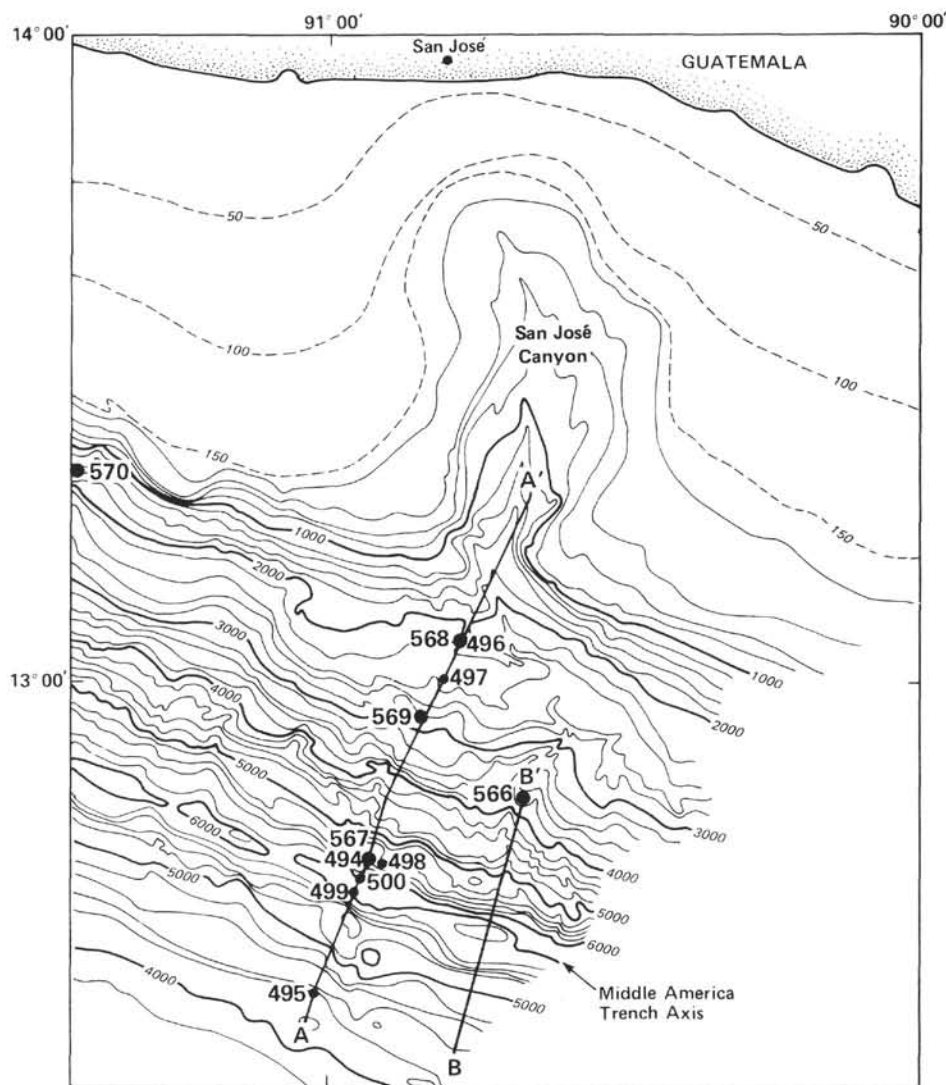


Figure 1. Location of Legs 84 and 67 sites off Guatemala. (Bathymetry is in meters.)

but shows normative corundum and a high water content, indicating its high level of alteration.

Trace Elements

Trace element composition of Sample 567A-19,CC is significantly different from that of the four other samples (Table 2). The former contains low amounts of Cr, Ni, Sr, Zr, Ba, and hygromagmaphile elements. In particular, its ratio $Ti/V = 20$ is close to that in orogenic lavas, according to Shervais (1982). Therefore, its trace element chemistry is nearly identical to that of Hole 494A samples previously studied by Maury et al. (1982); as these authors suggested for the Hole 494A samples, an orogenic parentage of the basalt of Sample 567A-19,CC seems to be indicated. Its extended Coryell-Masuda plot of REE (rare earth elements) and other hygromagmaphile elements (Fig. 2) shows the typical LREE (light rare earth elements) depleted pattern, similar to that of Hole 494A samples.

High amounts of Cr (≈ 200 ppm), Ni (≈ 100 ppm), Sr (242–425 ppm), Ba (113–265 ppm), and hygromag-

maphile elements characterize the four other basalts (Table 2). Their Ti/V ratios range from 57 to 102; so higher than 50, these ratios are symptomatic of an alkaline affinity (Shervais, 1982). The Coryell-Masuda patterns of two samples (Fig. 2) are typically LREE enriched. These results indicate that these rocks are clearly different from typical oceanic tholeiites from the Cocos Plate (Sites 495, 499, 500, DSDP Leg 67) as well as from Hole 494A samples.

The very high contents of Rb (43 ppm) and Cs (2.7 ppm) in Sample 567A-29-2, 147–149 cm (Table 2) are probably linked to secondary alteration processes.

MINERALOGY

Four samples (567A-19,CC; 567A-25-2, 90–96 cm; 567A-25-3, 74–78 cm, and 567A-26-1 (Piece 1, 3–4 cm) were studied with a Camebax-type automated microprobe (Microsonde Ouest, Brest—working conditions: 15 kV, 10 nA; counting time 6 s; oxide concentrations lower than 0.3% were not considered as representative).

Table 1. Major elements analysis (wt. %) and CIPW norms of Hole 567A basalts compared with an orogenic basalt from Hole 494A.

| Element | Sample (hole-core-section, interval in cm) | | | | | |
|--------------------------------|---|------------------|------------------|------------------|--------------------------|--------------------|
| | 567A-19,CC | 494A-29,CC (0-4) | 567A-25-2, 90-96 | 567A-25-3, 74-78 | 567A-26-1 (Piece 1, 3-4) | 567A-29-2, 147-149 |
| SiO ₂ | 50.80 | 51.88 | 42.85 | 42.35 | 44.20 | 46.10 |
| TiO ₂ | 0.64 | 0.35 | 2.62 | 2.59 | 2.57 | 2.29 |
| Al ₂ O ₃ | 16.41 | 14.60 | 14.80 | 14.95 | 14.02 | 17.25 |
| Fe ₂ O ₃ | 8.49 | 8.05 | 11.81 | 11.77 | 11.30 | 11.84 |
| MnO | 0.13 | 0.14 | 0.17 | 0.18 | 0.20 | 0.11 |
| MgO | 6.79 | 8.68 | 7.74 | 7.01 | 6.56 | 2.07 |
| CaO | 7.75 | 8.43 | 9.97 | 8.16 | 9.85 | 5.06 |
| Na ₂ O | 3.21 | 2.98 | 3.13 | 3.49 | 3.35 | 3.29 |
| K ₂ O | 0.51 | 0.47 | 0.47 | 0.43 | 0.57 | 1.69 |
| P ₂ O ₅ | 0.00 | 0.10 | 0.14 | 0.14 | 0.35 | 0.51 |
| Loss on ignition 1050°C | 4.22 | 3.32 | 4.68 | 5.14 | 2.71 | 5.76 |
| H ₂ O ⁻ | 0.64 | 0.79 | 2.15 | 3.02 | 3.89 | 3.46 |
| Total | 99.59 | 99.79 | 100.53 | 99.23 | 99.57 | 99.43 |
| Q | 1.02 | | | | | 2.92 |
| or | 3.21 | | 2.99 | 2.82 | 3.66 | 11.18 |
| ab | 28.88 | | 19.41 | 26.08 | 25.47 | 31.16 |
| an | 30.70 | | 26.91 | 26.48 | 23.39 | 24.75 |
| ne | | | 4.95 | 3.62 | 2.87 | |
| co | | | | | | 2.14 |
| di | wo 4.25 | | 10.66 | 7.32 | 11.45 | |
| | en 2.53 | | 6.40 | 4.26 | 6.63 | |
| | fs 1.50 | | 3.69 | 2.72 | 4.30 | |
| en | 15.45 | | | | | 5.77 |
| fs | 9.19 | | | | | 12.98 |
| fo | | | 10.08 | 10.59 | 7.79 | |
| fa | | | 6.41 | 7.45 | 5.57 | |
| mt | 1.96 | | 2.77 | 2.84 | 2.67 | 2.88 |
| il | 1.29 | | 5.37 | 5.46 | 5.30 | 4.87 |
| ap | 0.00 | | 0.36 | 0.37 | 0.90 | 1.35 |
| S.I. | 37.14 | | 34.96 | 32.30 | 31.46 | 11.62 |
| D.I. | 33.11 | | 27.36 | 32.52 | 32.00 | 45.26 |

Note: Fe₂O₃* = total iron as Fe₂O₃. The CIPW norms are calculated with 85% total iron as FeO and 15% as Fe₂O₃. D.I. = differentiation index; S.I. = solidification index. Analyses were done by J. Cotten, Brest. Blank spaces in CIPW norms mean absence of normative minerals or of calculated CIPW norm (Sample 494A-29,CC [0-4 cm]).

Table 2. Trace element analyses of Hole 567A samples (ppm).

| Sample (interval in cm) | Li | Ti | V | Cr | Mn | Fe | Co | | Ni | | Zn | Rb | | Sr | Zr | Sb | Cs | Ba | | La | Ce | Eu | Tb | Hf | Ta | Th | U |
|----------------------------|----|--------|-----|-----|------|---------|----|----|----|-----|-----|----|------|-----|-----|------|------|-----|-----|------|------|------|------|------|-------|------|------|
| | AA | AA | AA | AA | NA | AA | AA | NA | AA | NA | AA | AA | NA | AA | NA | NA | NA | AA | NA | AA | NA | NA | NA | NA | NA | NA | NA |
| 567A-19,CC | 13 | 3840 | 198 | 46 | 1830 | 10,6325 | 35 | 31 | 33 | 46 | 59 | 4 | 2.5 | 91 | 40 | 0.04 | 0.09 | 83 | 74 | 0.86 | 2.6 | 0.47 | 0.29 | 0.93 | 0.017 | 0.09 | 0.04 |
| 567A-25-2, 90-96 | 23 | 15,710 | 253 | 198 | 2395 | 14,7900 | 40 | 41 | 94 | 113 | 92 | 4 | 3.4 | 355 | 176 | 0.06 | 0.03 | 144 | 163 | 16.2 | 35.6 | 1.80 | 0.86 | 4.10 | 1.74 | 1.62 | 0.40 |
| 567A-25-3, 74-78 | 20 | 15,530 | 248 | 182 | 2535 | 14,7400 | 35 | 38 | 79 | 100 | 88 | 2 | 1.8 | 425 | 181 | 0.07 | 0.04 | 217 | 191 | 16.1 | 28.2 | 2.01 | 0.85 | 3.90 | 1.82 | 1.70 | 0.39 |
| 567A-26-1 (# 3-4) | | 15,410 | 268 | 193 | 2820 | 14,1515 | 30 | | 95 | | 90 | 11 | | 289 | | | | 113 | | | | | | | | | |
| 567A-29-2, 147-149 | 29 | 13,730 | 135 | 209 | 1550 | 14,8280 | 52 | 54 | 85 | 97 | 150 | 43 | 47.3 | 242 | 152 | 1.06 | 2.70 | 265 | 268 | 16.2 | 29.7 | 1.78 | 0.83 | 3.46 | 1.44 | 1.42 | 0.38 |

Note: AA = atomic absorption analysis (J. Cotten, Brest); NA = neutron activation analysis (J. L. Toron, Saclay). Blank spaces indicate no data available.

Pyroxenes

All the analyzed pyroxenes are Ca-rich clinopyroxenes (Table 3). Most of the phenocryst from Sample 567A-19,CC plot into the endiopside field (Fig. 3) and show high Mg/Fe ratios, high SiO₂, and low Al₂O₃ and TiO₂ contents (Table 3). The corresponding groundmass crystals restricted the iron-enrichment trend. In the discrimination diagram Ti/(Ca + Na) proposed by Leterrier et al. (1982) (Fig. 4A), the phenocryst plot into the field of tholeiitic and calc-alkalic pyroxenes. In the (Ti + Cr)/Ca diagram (Fig. 4B) of Leterrier et al. (1982), the clinopyroxenes clearly plot in the field of orogenic basalts, well outside the area of the field that overlaps

with the field of nonorogenic tholeiites. All these results are very similar to those obtained from Hole 494A pyroxenes (Maury et al., 1982).

The clinopyroxenes from the three other samples are clearly different: they are richer in iron relative to 567A-19,CC clinopyroxenes and plot near the augite/salite boundary or even in the salite field; their Al₂O₃ and TiO₂ contents are high. The phenocrysts show only restricted zoning patterns, and their rims and the groundmass crystals are slightly iron-enriched in comparison with their cores. In the discrimination diagram Ti/(Ca + Na) (Fig. 4A), the clinopyroxene phenocrysts plot within or near the field of pyroxenes from alkali basalts. The pyroxenes from the alkali basalts from the lower

Table 3. Representative clinopyroxene microprobe analyses (wt. %).

| Sample | Sample (hole-core-section, cm interval) | | | | | | | | | | | |
|--------------------------------|--|--------|--------|--------|-------|-------|------------------|-------|--------|--------|--------|--------|
| | 567A-19,CC | | | | | | 567A-25-2, 90-96 | | | | | |
| | C (1) | C (2) | C (3) | C (4) | C (5) | G (6) | G (7) | G (8) | C (9) | C (10) | G (11) | G (12) |
| SiO ₂ | 53.34 | 53.32 | 53.24 | 52.47 | 51.42 | 51.88 | 50.36 | 49.19 | 49.29 | 49.54 | 50.52 | 52.01 |
| TiO ₂ | 0.10 | 0.12 | 0.17 | 0.18 | 0.29 | 0.27 | 0.42 | 0.59 | 1.95 | 1.91 | 1.32 | 0.61 |
| Al ₂ O ₃ | 1.48 | 2.75 | 2.28 | 3.64 | 3.83 | 2.38 | 3.05 | 2.88 | 4.10 | 3.55 | 2.52 | 1.01 |
| Cr ₂ O ₃ | 0.08 | 0.20 | 0.22 | 0.10 | 0.19 | 0.00 | 0.01 | 0.00 | 0.05 | 0.00 | 0.00 | 0.00 |
| FeO* | 4.47 | 4.79 | 4.91 | 5.95 | 6.27 | 8.09 | 9.96 | 15.48 | 9.68 | 9.74 | 10.65 | 13.19 |
| MnO | 0.17 | 0.11 | 0.08 | 0.18 | 0.27 | 0.13 | 0.21 | 0.30 | 0.10 | 0.05 | 0.32 | 0.71 |
| MgO | 19.88 | 18.53 | 18.78 | 18.42 | 18.37 | 16.75 | 15.38 | 12.44 | 14.46 | 14.25 | 14.61 | 15.25 |
| CaO | 20.15 | 20.38 | 20.36 | 19.18 | 18.59 | 19.74 | 19.73 | 18.06 | 20.46 | 19.99 | 19.61 | 17.05 |
| Na ₂ O | 0.14 | 0.13 | 0.11 | 0.09 | 0.14 | 0.12 | 0.14 | 0.16 | 0.54 | 0.33 | 0.35 | 0.81 |
| Total | 99.81 | 100.83 | 100.15 | 100.21 | 99.37 | 99.36 | 99.26 | 99.10 | 100.63 | 99.36 | 99.90 | 100.14 |
| Ca | 39.18 | 40.77 | 40.41 | 38.68 | 37.75 | 39.92 | 40.21 | 37.87 | 42.43 | 42.13 | 40.43 | 34.71 |
| Mg | 53.78 | 51.57 | 51.86 | 51.67 | 51.89 | 47.10 | 43.61 | 36.30 | 41.72 | 41.77 | 41.91 | 43.20 |
| Fe + Mn | 7.04 | 7.65 | 7.73 | 9.65 | 10.36 | 12.98 | 16.18 | 25.83 | 15.85 | 16.10 | 17.66 | 22.09 |

Note: FeO* = total iron as FeO; positions are indicated by C = core of a phenocryst, R = rim of a phenocryst, and G = groundmass crystal; number in parenthesis = analysis number.

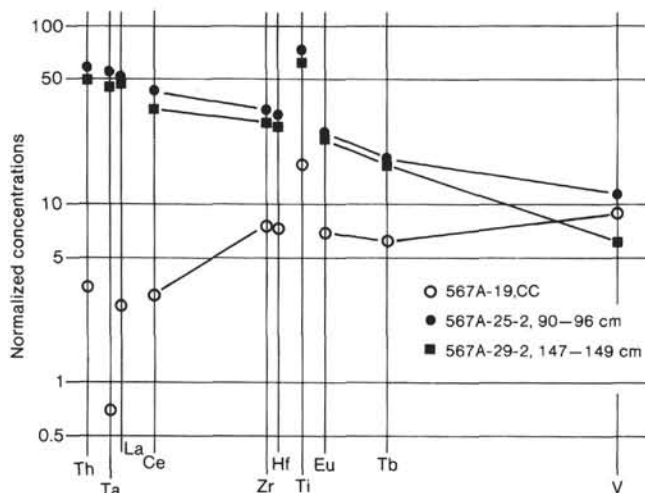


Figure 2. Extended Coryell-Masuda plots for selected samples from Hole 567A.

structural unit of the Santa Elena complex of Costa Rica (Azéma and Tournon, 1980) have a similar location in this diagram (Girard, 1981; Maury et al., 1982). It has been suggested that the Santa Elena complex is the onshore equivalent of the Hole 567A sequence (Aubouin et al., this volume; Bourgois et al., this volume).

Plagioclases

In Sample 567A-19,CC, groundmass plagioclase composition ranges from An₇₂ to An₅₀. As previously shown for Hole 494A samples (table 5 in Maury et al., 1982), the groundmass plagioclases do not contain significant amounts of K₂O and MgO and their composition differs from that of plagioclases from alkali basalts and oceanic tholeiites (Table 4).

In the three other basalts, the plagioclases (labrador to oligoclase) contain significant amounts of orthoclase (up to 10%). These characteristics are commonly found in plagioclases from alkali basalts. The phenocrysts range

in composition from An₆₉ to An₁₂ and show a normal zoning pattern with a progressive decrease of anorthite accompanied by an increase of orthoclase component toward their rims (Table 4 — Analyses 27 to 31 show the transition from andesine to potassic oligoclase). The groundmass plagioclase ranges in composition from An₆₇ to An₃₆.

Iron-Titanium Oxides

Chromiferous spinels (Analysis 35, Table 5) occur sporadically in Samples 567A-25-2, 90-96 cm; 567A-25-3, 74-78 cm; and 567A-26-1, (Piece 1, 3-4 cm). In the Al₂O₃/Cr₂O₃ diagram of Barbot (1983), these chromiferous spinels plot within the field of chromiferous spinels from alkaline basalts. These spinels are depleted in Cr and Al relative to spinels from oceanic basalts (Sigurdsson and Schilling, 1976). The hemoilmenites have retained much of their primary composition (Table 5, Analyses 38 to 40). On the other hand, the titanomagnetites have suffered various degrees of secondary oxidation and the sum of their oxides is always below 10%, when it is recalculated according to Carmichael's (1967) method. Despite these results, the compositions of coexisting titanomagnetites and hemoilmenites have been tentatively equilibrated following Powell and Powell's (1977) formulation of Buddington and Lindsley's (1964) geothermometer: all the available analyses from a given rock have been treated using a systematic combination as described by D'Arco et al. (1981). Temperatures range from 1200 to 900°C, with a maximum frequency around 1100 to 1000°C (Fig. 5); the corresponding oxygen fugacities values lie between the nickel-nickel oxide (NNO) and the fayalite-magnetite-quartz (FMQ) buffers.

⁴⁰K-⁴⁰Ar RADIOMETRIC DATA

EXPERIMENTAL PROCEDURE

Four samples—567A-19,CC; 567A-25-2, 90-96 cm; 567A-25-3, 74-78 cm; and 567A-29-2, 147-149 cm—were dated by the conventional ⁴⁰K-⁴⁰Ar method. Bulk rock samples were crushed into fragments of 0.15 to 0.30 mm in size and cleaned with distilled water to eliminate

Table 3. (Continued).

| Sample (hole-core-section, cm interval) | | | | | | | | | | | |
|--|--------|--------|--------|--------------------------|--------|--------|--------|--------|--------|--------|--------|
| 567A-25-3 74-78 | | | | 567A-26-1 (Piece 1, 3-4) | | | | | | | |
| C (13) | C (14) | G (15) | G (16) | C (17) | R (18) | C (19) | R (20) | C (21) | G (22) | G (23) | G (24) |
| 47.03 | 46.60 | 48.25 | 47.30 | 47.32 | 43.14 | 47.41 | 44.51 | 45.30 | 45.30 | 46.51 | 45.03 |
| 2.99 | 3.36 | 2.69 | 2.35 | 2.56 | 2.60 | 4.34 | 1.98 | 4.53 | 3.74 | 3.10 | 4.14 |
| 5.85 | 5.59 | 5.12 | 4.29 | 5.49 | 4.74 | 7.33 | 4.25 | 6.39 | 5.96 | 4.76 | 5.74 |
| 0.01 | 0.00 | 0.00 | 0.00 | 0.10 | 0.02 | 0.05 | 0.00 | 0.13 | 0.04 | 0.05 | 0.00 |
| 9.76 | 11.98 | 9.60 | 13.68 | 8.81 | 10.02 | 11.49 | 15.49 | 11.61 | 11.90 | 12.47 | 13.16 |
| 0.13 | 0.18 | 0.33 | 0.42 | 0.00 | 0.16 | 0.10 | 0.42 | 0.19 | 0.18 | 0.22 | 0.18 |
| 12.94 | 11.17 | 13.22 | 11.61 | 13.76 | 12.80 | 11.08 | 9.49 | 10.81 | 10.73 | 11.11 | 9.97 |
| 20.65 | 20.11 | 20.32 | 18.59 | 21.30 | 21.32 | 21.04 | 20.23 | 21.21 | 21.30 | 21.29 | 20.60 |
| 0.43 | 0.52 | 0.56 | 0.48 | 0.48 | 0.35 | 0.59 | 0.56 | 0.69 | 0.45 | 0.60 | 0.61 |
| 99.79 | 99.51 | 100.09 | 99.75 | 99.80 | 99.33 | 99.16 | 99.83 | 100.07 | 99.60 | 100.11 | 99.42 |
| 44.53 | 44.55 | 43.74 | 40.62 | 45.03 | 45.29 | 46.23 | 44.12 | 46.66 | 46.66 | 45.63 | 45.91 |
| 38.83 | 34.41 | 39.58 | 35.31 | 40.44 | 37.84 | 33.88 | 28.78 | 33.07 | 32.69 | 33.13 | 30.91 |
| 16.64 | 21.04 | 16.68 | 24.07 | 14.53 | 16.87 | 19.89 | 27.10 | 20.27 | 20.65 | 21.24 | 23.18 |

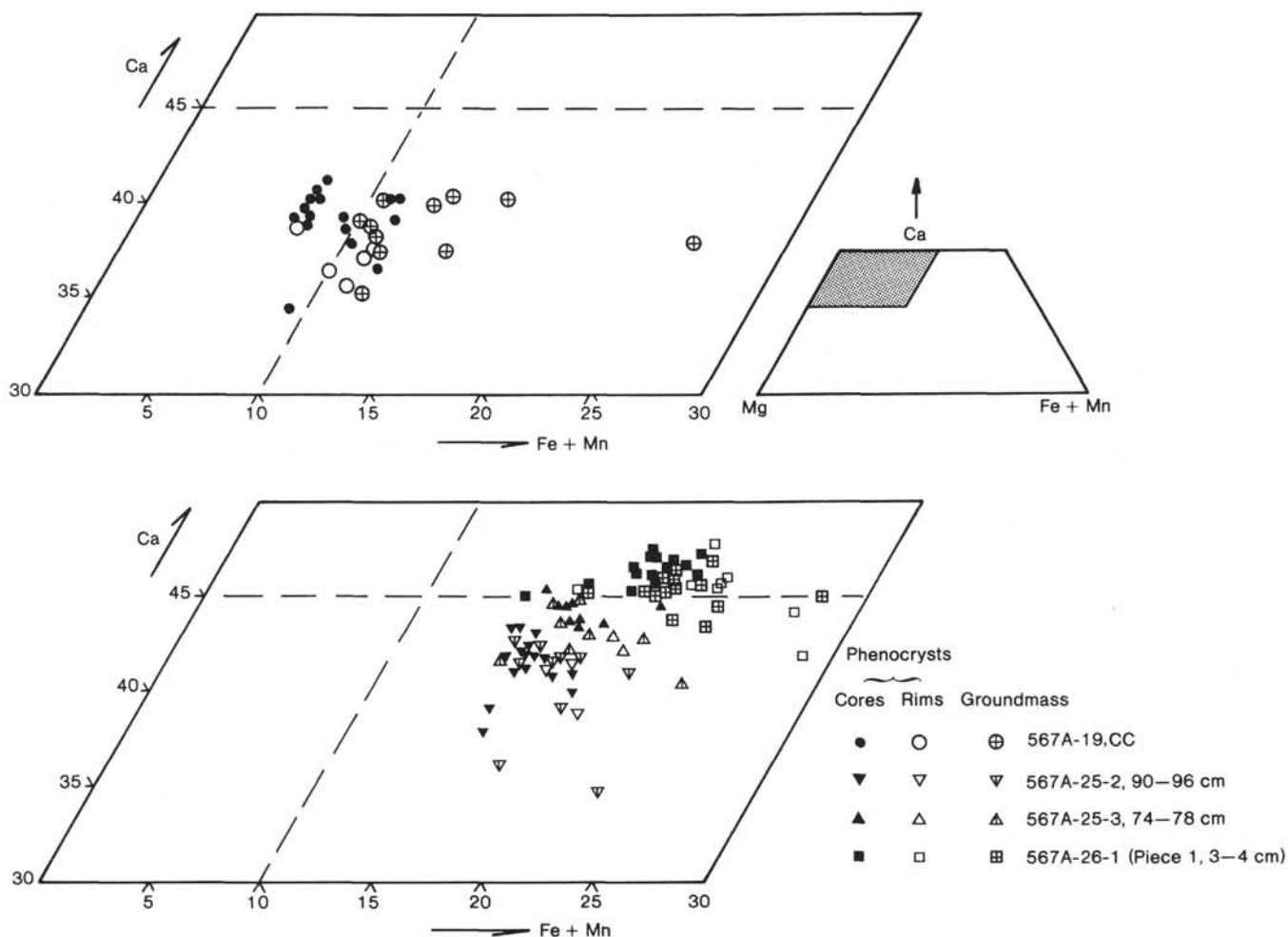


Figure 3. Clinopyroxene compositions plotted on Ca-Mg-(Fe + Mn) diagram.

the crushing powder adhering to the grains; grains were picked by hand (Sample 567A-29-2, 147-149 cm) when calcite was too abundant in the groundmass. An aluminum-foil target containing a known volume of ^{38}Ar buried as positive ions under a 30-kV energy (Bellon et al., 1981) was added to each sample at time of weighing and was used as a spike. After fusion in a molybdenum crucible heated by induc-

tion, gases released from the sample were cleaned on three titanium sponge furnaces, and purification was achieved with a titanium-zirconium getter. Isotopic analyses were done using isotopic dilution in a 180° and 6-cm radius mass spectrometry running in static mode. The permanent magnetic field was 3300 gauss, and the ion accelerating voltage between 500 and 600 volts. Mass discrimination correction was

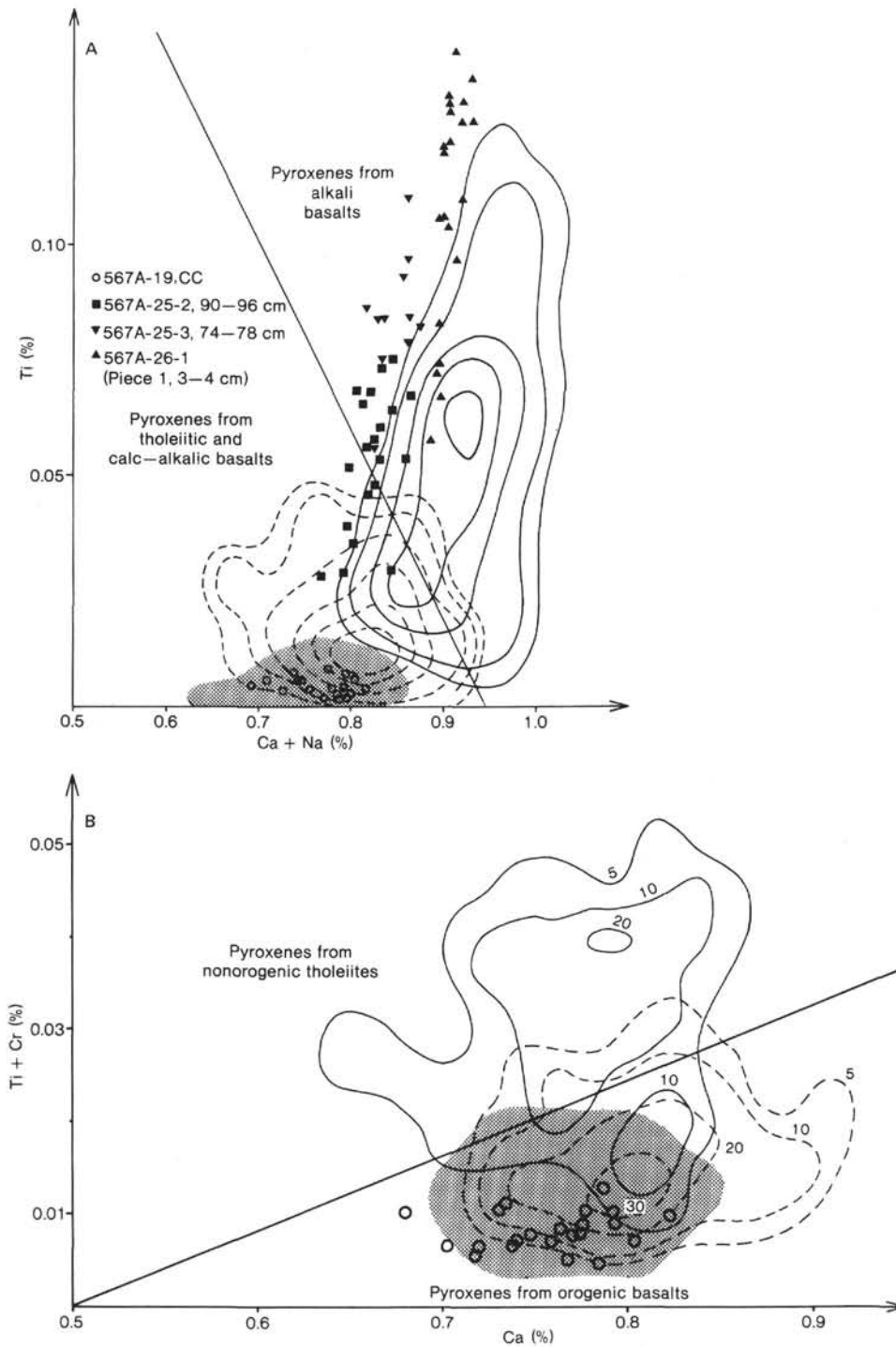


Figure 4. Plot of clinopyroxene phenocryst composition on Leterrier et al. (1982) diagrams. Gray area indicates plot of clinopyroxene phenocryst composition in orogenic lavas from Hole 494A. A. Ti/(Ca + Na) diagram. B. (Ti + Cr)/Ca diagram.

applied after each analysis, using air argon standards within the argon compositional range of each sample. Table 6 provides age results.

Results and Discussion

Sample 567A-19,CC indicates an age of 78.7 ± 3.9 m.y. Beyond the formation of secondary calcite and chlo-

rite in glassy parts of the sample, our geochemical and mineralogical studies detected no major alteration products in this basalt, such as K_2O enrichment or/and a large developed secondary mineralogical paragenesis, both linked to seawater weathering. Therefore the age of 78.7 m.y. may be considered valid or at least close to the

Table 4. Plagioclase analyses (microprobe) for Sample 567A-25-2, 90-96 cm (wt. %).

| | Position (analysis number) | | | | | | | | | |
|----------------------------------|----------------------------|--------|--------|--------|--------|--------|--------|--------|--------|--------|
| | C (25) | R (26) | C (27) | C (28) | C (29) | C (30) | R (31) | G (32) | G (33) | G (34) |
| SiO ₂ | 54.54 | 61.20 | 66.49 | 57.15 | 59.11 | 61.28 | 65.29 | 53.11 | 54.64 | 58.10 |
| Al ₂ O ₃ | 27.69 | 23.53 | 27.27 | 26.21 | 25.04 | 23.45 | 20.11 | 28.97 | 27.70 | 25.49 |
| Fe ₂ O ₃ * | 0.64 | 0.70 | 0.62 | 0.71 | 0.48 | 0.39 | 0.38 | 0.82 | 0.64 | 0.82 |
| CaO | 10.27 | 5.29 | 9.36 | 7.94 | 6.70 | 5.11 | 2.60 | 11.69 | 9.93 | 7.52 |
| Na ₂ O | 5.55 | 8.18 | 6.37 | 6.77 | 7.56 | 8.47 | 8.97 | 4.77 | 5.84 | 6.93 |
| K ₂ O | 0.32 | 0.70 | 0.31 | 0.36 | 0.62 | 0.72 | 1.67 | 0.20 | 0.33 | 0.50 |
| Total | 99.01 | 99.60 | 100.42 | 99.14 | 99.41 | 99.42 | 99.02 | 99.56 | 99.08 | 99.36 |
| Ca | 49.7 | 25.3 | 44.1 | 38.5 | 31.9 | 24.0 | 12.5 | 56.8 | 47.5 | 36.4 |
| Na | 48.5 | 70.7 | 54.2 | 59.4 | 65.2 | 72.0 | 78.0 | 42.0 | 50.6 | 60.7 |
| K | 1.8 | 4.0 | 1.7 | 2.1 | 2.9 | 4.0 | 9.5 | 1.2 | 1.9 | 2.9 |

Note: Position is indicated by C = core of phenocryst, R = rim of phenocryst, and G = groundmass crystal; number in parenthesis = analysis number. Fe₂O₃* = total iron as FeO. The sizes of plagioclase phenocrysts 25 and 26 and 27 through 31 are 150 μm and 450 μm, respectively.

Table 5. Analyses of chromite (CHR), titanomagnetite (MT), and coexisting hemoilmenite (IL), and of secondary minerals, chlorite (CHL), celadonite (CE), and albite (AB), (wt. %).

| Mineral | Sample (interval in cm) | | | | | | | | | | |
|--------------------------------|-----------------------------|---------|------------------|---------|---------|---------|----------------------|---------|--------------------------|---------|--|
| | 567A-26-1 (Piece 1, 3-4) | | 567A-25-2, 90-96 | | | | 567A- 25-2, 90-96 | | 567A-26-1 (Piece 1, 3-4) | | |
| | CHR (35) | MT (36) | MT (37) | IL (38) | IL (39) | IL (40) | CHL (41) | CE (42) | CE (43) | AB (44) | |
| SiO ₂ | 0.00 | 0.05 | 0.08 | 0.08 | 0.00 | 0.00 | 33.68 | 54.44 | 54.28 | 67.82 | |
| TiO ₂ | 5.43 | 22.00 | 23.32 | 48.55 | 48.29 | 49.42 | 0.01 | 0.02 | 0.13 | 0.00 | |
| Al ₂ O ₃ | 16.21 | 1.35 | 1.23 | 0.15 | 0.10 | 0.26 | 14.82 | 5.59 | 7.87 | 20.80 | |
| Cr ₂ O ₃ | 26.15 | 0.00 | 0.05 | 0.00 | 0.00 | 0.00 | 0.00 | 0.00 | 0.00 | 0.02 | |
| Fe ₂ O ₃ | 17.40 | 22.84 | 20.66 | 8.56 | 10.31 | 8.07 | | | | 0.08 | |
| FeO | 20.02 | 47.73 | 48.71 | 89.49 | 39.19 | 38.75 | 19.36 | 17.23 | 15.93 | | |
| MnO | 0.30 | 3.01 | 3.37 | 0.69 | 0.65 | 0.70 | 0.00 | 0.00 | 0.00 | 0.00 | |
| MgO | 6.76 | 0.00 | 0.00 | 2.00 | 2.04 | 2.90 | 18.76 | 6.11 | 6.02 | 0.04 | |
| CaO | 0.00 | 0.07 | 0.03 | 0.07 | 0.09 | 0.07 | 0.45 | 0.08 | 0.22 | 0.24 | |
| Na ₂ O | 0.06 | 0.00 | 0.00 | 0.06 | 0.00 | 0.09 | 0.16 | 0.04 | 0.06 | 10.09 | |
| K ₂ O | 0.00 | 0.00 | 0.02 | 0.03 | 0.02 | 0.03 | 0.06 | 10.51 | 10.72 | 0.03 | |
| Total | 101.35 | 97.05 | 97.47 | 99.68 | 100.69 | 100.29 | 87.30 | 94.02 | 95.23 | 99.12 | |
| Usp (%) | | 65.8 | 69.3 | | | | | | | | |
| He (%) | | | | 8.1 | 9.6 | 7.6 | | | | | |
| FM | 0.71 | | | | | | 0.37 | 0.61 | 0.60 | | |

Note: Numbers in parentheses = analysis numbers. Total iron as Fe₂O₃ for albite, FeO for chlorite and celadonite; distributed by R₃O₄ and R₂O₃ stoichiometry for spinel and ilmenite, respectively. For ulvöspinel (Usp) and hematite (He), molar percentages are calculated following Carmichael's (1967) method. FM = FeO* + MnO/MgO + FeO* + MnO.

true crystallization age of the orogenic lava. This age is in good agreement from the same stratigraphic position at the bottom of upper Campanian - lower Maestrichtian limestones—around 72 ± 1 m.y., according to Odin and Kennedy (1982).

For the three other lavas with alkaline affinities, the radiometric results are scattered and probably reflect the effects of alteration and its contribution to the potassium budget of each sample, either through a secondary K₂O enrichment in the groundmass or on the rim of plagioclase phenocryst or through a secondary K₂O depletion of the original whole rock linked to the development of K₂O-poor minerals. A correlation appears between the loss on ignition (1050°C) and the age of each sample. The youngest radiometric age (91 ± 4.5 m.y.) was obtained for Sample 567A 29-2, 147-149 cm, which gave the highest L.O.I. (loss on ignition—1050°C) (5.76%). Sample 567A-25-3, 74-78 cm with a L.O.I. of

5.14%, has an intermediate radiometric age of 132 ± 6.6 m.y. The oldest age (169 ± 8.4 m.y.), of Sample 567A-25-2, 90-96 cm corresponds to a L.O.I. of 4.68%.

In the latter two samples, the K₂O contents (0.43 and 0.47—see Table 6) and the trace elements data (Rb, 2 and 4 ppm; Cs, below 0.05 ppm) indicate no strong variations. A large modification of the primary potassium budget seems unlikely, but considering the volume of secondary K₂O-poor minerals in the samples, it appears that the oldest radiometric age is obtained from the basalt in which the secondary paragenesis is less developed, compared to the youngest one where chlorite is abundant. The youngest age (91 m.y.) of Sample 567A 29-2, 147-149 cm which is a probable pillow-rim, is attributed at least in part to a strong enrichment in K₂O (1.69%) accompanied by high values of Rb and Cs contents (43 and 2.7 ppm respectively), and perhaps to continual loss of a radiogenic argon because of the low re-

Table 6. $^{40}\text{K} - ^{40}\text{Ar}$ radiometric analyses.

| Description | Sample (interval in cm) | Age (m.y.) (\pm uncertainty) | $^{40}\text{Ar}^*$ ($10^{-7} \text{ cm}^3/\text{g}$) | K_2O (%) | Weight (g) | % $\frac{^{40}\text{Ar}^*}{^{40}\text{Ar}_T}$ | Exp. number | |
|--------------------------|-------------------------|---------------------------------|--|--------------------------|------------|---|-------------|------|
| Porphyritic basalt | 567A-19,CC | 78.7 ± 3.9 | 77.6 | 13.12 | 0.51 | 0.9839 | 71.7 | B.77 |
| | | | 79.9 | 13.52 | 0.51 | 0.9773 | 69.1 | B.76 |
| Coarse-grained dolerites | 567A-25-2, 9-96 | 169 ± 8.4 | 168 | 26.84 | 0.47 | 1.0053 | 68.3 | B.74 |
| | | | 170 | 27.28 | 0.47 | 1.0021 | 70.6 | B.75 |
| Quenched texture | 567A-25-3, 74-78 | 132 ± 6.6 | 132 | 19.17 | 0.43 | 1.0127 | 82.6 | B.78 |
| | | | 91 | 51.29 | 1.69 | 0.9941 | 50 | B.80 |

Note: $^{40}\text{Ar}^*$ signifies radiogenic argon. Ages are calculated following the relation: time (in m.y.) = $4153.9 \log_{10} (1 + 142.33 \frac{^{40}\text{Ar}^*}{\text{K}})$ calculated with the constants by Steiger and Jäger (1977). Uncertainties are estimated to be $\pm 5\%$ of the calculated age. Ages in braces are the results of two independent determinations carried out on the sample. In the $\frac{^{40}\text{Ar}^*}{^{40}\text{Ar}_T}$ relation, $^{40}\text{Ar}_T$ signifies total ^{40}Ar (i.e., radiogenic $^{40}\text{Ar}^*$ and atmospheric ^{40}Ar). Exp. number = experiment number.

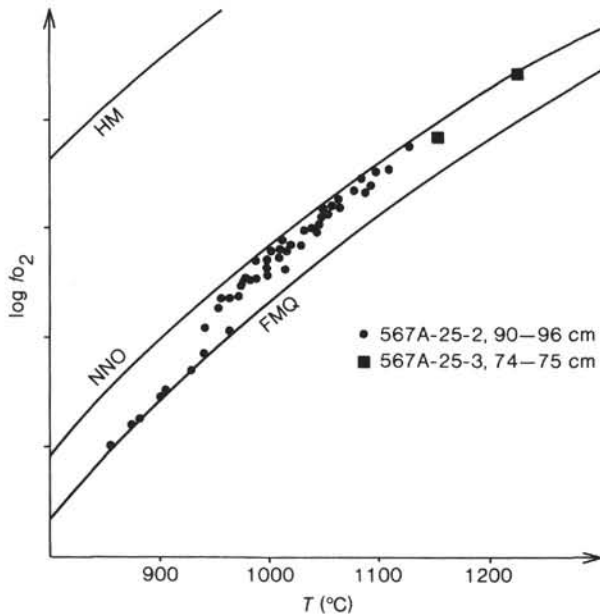


Figure 5. Temperature-oxygen fugacity (T - f_{O_2}) diagram for coexisting iron-titanium oxides. NNO = nickel-nickel oxide; FMQ = fayalite-magnetite-quartz buffer; HM = hematite-magnetic buffer.

tention of some of the potassium sites. In this sample, the radiogenic/total argon ratio (Table 6) is significantly lower (0.50), whereas its K_2O content is three times greater than that of the two other samples. Their argon ratios average 0.7 to 0.8.

We may retain the significant difference between the age of the orogenic lava and the ages (132–168 m.y.) of the alkaline lavas, which we must consider with caution. These must be analyzed for comparison with ages obtained from numerous samples of the onshore complex of Santa Elena, and substantiated by paleontological data. In particular, some radiometric ages around 130 m.y. have been determined on potassic alkaline rocks from the lower structural unit of the complex (Bellon et al. unpublished data).

CONCLUSIONS

1. Sample 567A-19,CC, which is stratigraphically analogous to the Hole 494A basalts, is similar to these basalts, and most of their mineralogical and geochemical

characteristics favor an orogenic affinity. Thus the radiometric age of 78.7 ± 3.9 m.y. may represent the age of cooling.

2. The four other samples are clearly different from 567-19,CC orogenic basalt and from the oceanic basalts from the Cocos Plate. Their geochemical tendencies (enrichment in light rare earths, Ba, Sr, and Ti, and the presence of normative nepheline) and their mineralogical features (pyroxenes and plagioclases) indicate that these rocks are alkaline basalts. They may be compared to those occurring in the lower unit from the Santa Elena complex. Their radiometric ages are older, although scattered results may reflect the effects of secondary alteration, and their ages might actually be much greater.

3. It is suggested (Aubouin et al., this volume) that Leg 84 basement sequences are equivalent to those of the Santa Elena complex. Our study indicates that basement ages may support this interpretation.

ACKNOWLEDGMENTS

R. J. Stern and Stephan Nelson reviewed this chapter; the authors wish to thank them for suggesting improvements in the manuscript.

REFERENCES

- Azéma, J., and Tournon, J., 1980. La péninsule de Santa-Elena, Costa-Rica: un massif ultrabasique charrié en marge pacifique de l'Amérique Centrale. *C.R. Acad. Sci. Paris*, 290:9–12.
- Barbot, J., 1983. Le nickel dans les olivines et les spinelles des roches basiques et ultrabasiques [Thesis]. Université de Bretagne Occidentale, Brest.
- Bellon, H., Quoc Buü, N., Chaumont, J., and Philippet, J. C., 1981. Implantation ionique d'argon dans une cible-support: application au traçage isotopique de l'argon contenu dans les minéraux et les roches. *C.R. Acad. Sci. Paris*, 292:977–980.
- Buddington, A. F., and Lindsley, D. H., 1964. Iron-titanium oxide minerals and synthetic equivalents. *J. Petrol.*, 5:310–357.
- Carmichael, I. S. E., 1967. The iron-titanium oxides of salic volcanic rocks and their associated ferromagnesian silicates. *Contrib. Mineral. Petrol.*, 14:36–64.
- D'Arco, Ph., Maury, R. C., and Westercamp, D., 1981. Geothermometry and geobarometry of a cummingtonite-bearing dacite from Martinique, Lesser Antilles. *Contrib. Mineral. Petrol.*, 77:177–184.
- Girard, D., 1981. Pétrologie de quelques séries spilitiques mésozoïques de la zone caraïbe et des ensembles magmatiques de l'île de Tobago: implications géodynamiques [Thesis]. Université de Bretagne Occidentale, Brest.
- Leterrier, J., Maury, R. C., Thonon, P., Girard, D., and Marchal, M., 1982. Clinopyroxene compositions as a method of identification

- of the magmatic affinities of paleo-volcanic series. *Earth Planet. Sci. Lett.*, 4:33-38.
- Maurly, R. C., Bougault, H., Joron, J. L., Girard, D., Treuil, M., Azéma, J., and Aubouin, J., 1982. Volcanic rocks from Leg 67 sites: mineralogy and geochemistry. In Aubouin, J., von Huene, R. et al., *Init. Repts., DSDP, 67*: Washington (U.S. Govt. Printing Office), 557-576.
- Odin, G. S., and Kennedy, W. J., 1982. Mise à jour de l'échelle des temps mésozoïques. *C.R. Acad. Sci. Paris*, 294:383-386.
- Powell, R., and Powell, M., 1977. Geothermometry and oxygen barometry using coexisting iron-titanium oxides: a reappraisal. *Mineral. Mag.*, 41:257-263.
- Shervais, J. W., 1982. Ti-V plots and the petrogenesis of modern and ophiolitic lavas. *Earth Planet. Sci. Lett.*, 59:101-118.
- Sigurdsson, H., and Schilling, J.-G., 1976. Spinels in Mid-Atlantic Ridge basalts: chemistry and occurrence. *Earth Planet. Sci. Lett.*, 29:7-20.
- Steiger, R. H., and Jäger, E. 1977. Subcommittee on geochronology: convention on the use of decay constants in geo and cosmochronology. *Earth Planet. Sci. Lett.*, 26:359-362.

Date of Initial Receipt: 7 April 1984

Date of Acceptance: 23 August 1983